

# Synthesis, Structure, and Electronic and Photophysical Properties of Two- and Three-Layered [3.3]Paracyclophane-Based Donor–Acceptor Systems<sup>1</sup>

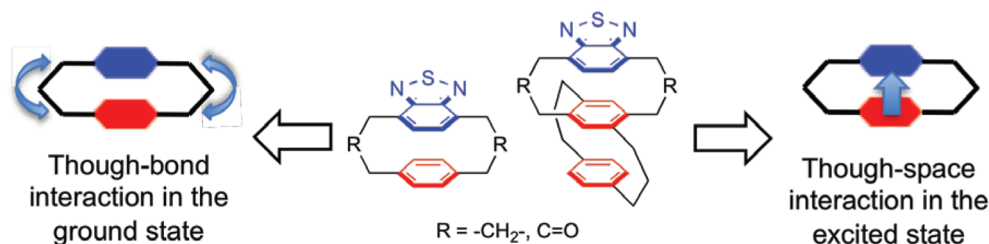
Motonori Watanabe,<sup>†,‡</sup> Kenta Goto,<sup>†</sup> Masahiko Shibahara,<sup>§</sup> and Teruo Shinmyozu<sup>\*,†</sup>

<sup>†</sup>Institute for Materials Chemistry and Engineering (IMCE), and <sup>‡</sup>Department of Chemistry, Graduate School of Sciences, Kyushu University, 6-10-1 Hakozaki, Higashi-ku, Fukuoka 812-8581, Japan, and

<sup>§</sup>Department of Chemistry, Faculty of Education and Welfare Science, Oita University, 700 Dannoharu, Oita 870-1192, Japan

shinmyo@ms.ifoc.kyushu-u.ac.jp

Received April 29, 2010



The synthesis, structural, redox, and photophysical properties of the two- and three-layered donor–acceptor (D–A) type [3.3]paracyclophanes ([3.3]PCPs) are described. The synthesis of the two- and three-layered [3.3]PCPs **1** and **2** containing 2,1,3-benzothiadiazole (BT) as an acceptor was achieved by the (*p*-ethylbenzenesulfonyl)methyl isocyanide coupling method. The cyclic voltammograms of **1** and **2** along with those of respective dione precursors **5** and **7** clearly indicate that the presence of the  $-\text{CH}_2\text{COCH}_2-$  bridge interferes with the electronic interactions between the BT and the benzene rings, suggesting the importance of the through-bond interaction in the ground state. In sharp contrast, the UV/vis spectra of **1** and **5** as well as those of **2** and **7** exhibit similar bands regardless of the presence of the  $-\text{CH}_2\text{COCH}_2-$  or  $-\text{CH}_2\text{CH}_2\text{CH}_2-$  bridges, indicating that the charge-transfer (CT) interaction is mainly responsible for the through-space interaction. The two-layered PCPs, **5** and **1**, show broad structureless fluorescence bands at the same position of 468 nm, while those of the three-layered PCPs, **7** and **2**, appear at 501 and 496 nm, respectively, with lower quantum yields compared to those of the two-layered PCPs probably due to the stronger intramolecular CT interaction of the three-layered PCPs in the ground state.

## 1. Introduction

Charge transfer (CT) and charge delocalization are important phenomena for molecular devices, whose structures are mainly divided into the  $\pi$ -conjugation type and  $\pi$ -stacked type. The  $\pi$ -conjugation type, which can modify the molecular sequence of the donor (D), bridge (B), and acceptor (A)

such as the D–A–D<sup>2</sup> and D–B–A systems<sup>3</sup> for organic molecular wires, has been widely studied and has made components available for the initial phase of developing molecules devices. On the other hand,  $\pi$ -stacked type molecular devices have been mainly studied in connection to DNA<sup>4</sup> and

(1) Donor–Bridge–Acceptor System. 1.  
(2) Balzani, V.; Credi, A.; Venturi, M. In *Molecular Devices and Machines*; Wiley-VCH: New York, 2008; pp 33–63.  
(3) (a) Paddon-Row, M. *Acc. Chem. Res.* **1994**, *27*, 18–25. (b) Jordan, K. D.; Paddon-Row, M. *Chem. Rev.* **1992**, *92*, 395–410. (c) Gust, D.; Moore, T. A.; Moore, A. L. *Acc. Chem. Res.* **1993**, *26*, 198–205. (d) James, D. K.; Tour, J. M. *Top. Curr. Chem.* **2005**, *257*, 33–62. (e) Weiss, E. A.; Wasielewski, M. R.; Ratner, M. R. *Top. Curr. Chem.* **2005**, *257*, 103–133.

(4) (a) Murphy, C. J.; Arkin, M. R.; Jenkins, Y.; Ghatlia, N. D.; Bossmann, S. H.; Turro, N. J.; Barton, J. K. *Science* **1993**, *262*, 1025–1029. (b) Kelley, S. O.; Barton, J. K. *Science* **1999**, *283*, 375–381. (c) Lewis, F.; Letsinger, R. L.; Wasielewski, M. R. *Acc. Chem. Res.* **2001**, *34*, 159–170. (d) Giese, B. *Annu. Rev. Biochem.* **2002**, *71*, 51–70. (e) Takada, T.; Kawai, K.; Fujitsuka, M.; Majima, T. *Chem.—Eur. J.* **2005**, *11*, 3835–3842. (f) Boussicault, F.; Robert, M. *Chem. Rev.* **2008**, *108*, 2622–2645. (g) Vura-Weis, J.; Wasielewski, M. R.; Thazhathveetil, A. K.; Lewis, F. D. *J. Am. Chem. Soc.* **2009**, *131*, 9722–9727.

polymers<sup>5</sup> but only a limited number of synthetic molecules of the loose  $\pi$ -stack type have been developed such as the oligophenylureas<sup>6</sup> and fluorenes.<sup>7</sup>

In previous papers, we reported the electron-donating ability of the multilayered [3.3]paracyclophanes (PCPs)<sup>8a,b</sup> and metacyclophanes (MCPs)<sup>8c-e</sup> using the wavelength ( $\lambda_{\max}$ ) of the CT band between a cyclophane ( $\pi$ -donor) and tetracyanoethylene (TCNE;  $\pi$ -acceptor) in  $\text{CHCl}_3$  or  $\text{CH}_2\text{Cl}_2$  (donor/acceptor = 1:1), which indicated that the  $\lambda_{\max}$ 's of the CT bands correlate well with the half-wave oxidation potentials ( $E_{1/2}$ ) of the cyclophanes, and the paracyclophanes [ $\lambda_{\max}$  606 (two-layered) to 723 nm (four) in  $\text{CHCl}_3$ ] show a greater electron-donating ability than that of the corresponding metacyclophanes [ $\lambda_{\max}$  509 (two-layered) to 588 nm (six) in  $\text{CHCl}_3$ ]. A significant increase in the electron-donating ability of the multilayered [3.3]PCPs with an increase in the layer (up to four), as well as transannular distances of the benzene rings (3.2–3.3 Å) similar to those of the base pairs of the double-strand structure of DNA (ca. 3.4 Å), prompted us to study the use the multilayered [3.3]PCPs as a bridge (B) of  $\pi$ -stacked type molecular wires as a mimic of the DNA-based one.<sup>4</sup> In the D–B–A-type molecular wire with the multilayered [3.3]PCP as a bridge, different electron-transfer and charge-transfer mechanisms may be observed compared to the corresponding mechanisms of the DNA-based ones.

Thus, we planned to synthesize the D–B–A molecules with the multilayered [3.3]PCP as a bridge. In the first step of this study, benzene and 2,1,3-benzothiadiazole (BTD) were chosen as the donor and acceptor, respectively. BTD as an acceptor not only has a high electron affinity<sup>9</sup> but also an ionization potential<sup>10</sup> similar to that of benzene. Our recent study on the BTD dimers, i.e., the *syn*- and *anti*-[2.2](4,7)-benzothiadiazolophanes, exhibited the formation of a radical anion species by pulse radiolysis<sup>11</sup> and  $\gamma$ -ray irradiation.<sup>12</sup> The magnitude of the electron delocalization between the two BTD rings was evaluated by the wavelength of the charge resonance band of the transient absorption spectrum of the radical anion species, and the *syn* isomer showed much

more significant electron delocalization than the *anti*-one.<sup>13</sup> The generation of the intramolecular dimer radical cations<sup>14</sup> and anions<sup>15</sup> of multibridged [3<sub>n</sub>]cyclophanes ( $n = 2-6$ ) and their relative stabilities were also studied by us. Properties of the multilayered [3.3]PCP-based molecular wire may be evaluated by the magnitude of the electron and charge delocalization as well as analysis of its transient absorption spectrum.

The rigid  $\pi$ -stack type donor–acceptor (D–A) molecules were mainly studied by Staab et al. and Misumi et al. with the two- to four-layered D–A PCPs, such as quinhydrone,<sup>16a-c</sup> quinone–porphyrin,<sup>16d,e</sup> TCNB–phane,<sup>16f,g</sup> and TCNQ–phane.<sup>16i,j</sup> In the multilayered D (1,4-dimethoxybenzene)–A (*p*-benzoquinone) [2.2]PCPs, in which two benzene rings are replaced by D and A, the CT stabilization was mainly attributed to the  $\pi$ -basicity of the durene ring which faces the acceptor quinone ring, and no orientation dependence of the D–A moieties on CT transition was observed.<sup>16h</sup> The magnitude of transannular electronic interaction, and accordingly the relationship between the magnitude of the CT interaction and the relative D–A orientation, was evaluated and discussed solely based on the CT absorption spectra. Therefore, a more detailed evaluation of the transannular electronic interaction and the stability of the radical anion and radical cation species is required, when using the  $\pi$ -stacked D–A type molecules as model compounds for designing molecular devices. We now report here the structural, redox, and photophysical properties of BTD containing D–A [3.3]PCPs, which are the smallest models of the rigid  $\pi$ -stacked D–A systems.

## 2. Results and Discussion

**Synthesis.** The synthesis of the two- and three-layered [3.3]PCPs **1** and **2** was achieved by the (*p*-ethylbenzenesulfonyl)-methyl isocyanide (EbsMIC) coupling method (Scheme 1).<sup>8a</sup> The chloride **3**<sup>17</sup> was coupled with the EbsMIC adduct **4**<sup>8a</sup> to give the two-layered PCP dione **5** (36%), which was converted by the Wolff–Kishner (WK) reduction to the corresponding two-layered [3.3]PCP **1** (57%). Similarly, the coupling of the chloride **3** and the two-layered EbsMIC adduct **6**<sup>8a</sup> (racemic) provided the three-layered PCP-dione **7** (racemic) (43%). The WK reduction of the carbonyl groups of **7** afforded the three-layered [3.3]PCP **2** (racemic, 64%).

All the aromatic proton signals of the two- and three-layered [3.3]PCPs show upfield shifts as the numbers of layers

(5) (a) Nakano, T.; Yade, T.; Yokoyama, M.; Nagayama, N. *Chem. Lett.* **2004**, *33*, 296–297. (b) Nakano, T.; Yade, T. *J. Am. Chem. Soc.* **2003**, *125*, 15474–15484. (c) Morisaki, Y.; Murakami, T.; Sawamura, T.; Chujo, Y. *Macromolecules* **2009**, *42*, 3656–3660.

(6) (a) Zeida, T. A.; Wang, Q.; Fiebig, T.; Lewis, F. D. *J. Am. Chem. Soc.* **2007**, *129*, 9848–9849. (b) Lewis, F. D.; Daublain, P.; Santos, G. B. D.; Liu, W.; Asatryan, A. M.; Markarian, S. A.; Fiebig, T.; Raychev, M.; Wang, Q. *J. Am. Chem. Soc.* **2006**, *128*, 4792–4801.

(7) (a) Rathore, R.; Abdelwahed, S. H.; Guzei, I. A. *J. Am. Chem. Soc.* **2003**, *125*, 8712–8713. (b) Nakano, T.; Yade, T. *Chem. Lett.* **2008**, *37*, 258–259.

(8) (a) Shibahara, M.; Watanabe, M.; Iwanaga, T.; Matsumoto, T.; Ideta, K.; Shinmyozu, T. *J. Org. Chem.* **2008**, *73*, 4433–4442. (b) Atsuya, M.; Shibahara, M.; Watanabe, M.; Matsumoto, T.; Shinmyozu, T.; Kobayashi, N. *J. Org. Chem.* **2008**, *73*, 9125–9128. (c) Shibahara, M.; Watanabe, M.; Iwanaga, T.; Ideta, K.; Shinmyozu, T. *J. Org. Chem.* **2007**, *72*, 2865–2877. (d) Shibahara, M.; Watanabe, M.; Aso, K.; Shinmyozu, T. *Synthesis* **2008**, *23*, 3749–3754. (e) Shibahara, M.; Watanabe, M.; Suenaga, M.; Ideta, K.; Matsumoto, T.; Shinmyozu, T. *Tetrahedron Lett.* **2009**, *50*, 1253–1260.

(9) Akhtaruzzaman, Md.; Tomura, M.; Nishida, J.; Yamashita, Y. *J. Org. Chem.* **2004**, *69*, 2953–2958.

(10) Clark, P. A.; Gleiter, R.; Hilbronner, E. *Tetrahedron* **1973**, *29*, 3085–3089.

(11) Fujita, M.; Ishida, A.; Majima, T.; Takamuku, S. *J. Phys. Chem.* **1996**, *100*, 5382–5387.

(12) Shida, T. *Electronic Absorption Spectra of Radical Ions*; Elsevier: Amsterdam, 1988.

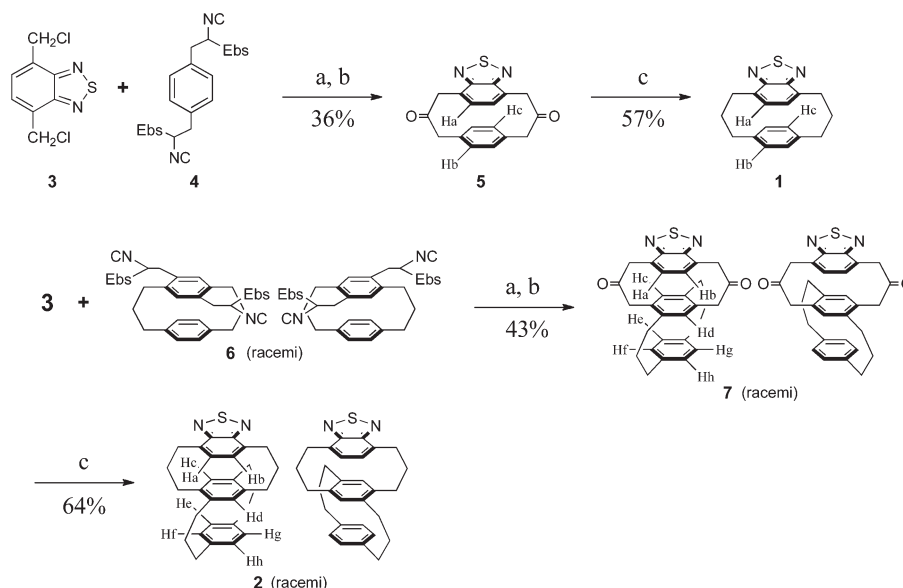
(13) Watanabe, M.; Goto, K.; Fujitsuka, M.; Tojo, S.; Majima, T.; Shinmyozu, T. *Bull. Chem. Soc. Jpn.*, in press.

(14) (a) Fujitsuka, M.; Samori, S.; Hara, M.; Tojo, S.; Yamashiro, S.; Shinmyozu, T.; Majima, T. *J. Phys. Chem. A* **2005**, *109*, 3531–3534. (b) Fujitsuka, M.; Cho, D. W.; Tojo, S.; Yamashiro, S.; Shinmyozu, T.; Majima, T. *J. Phys. Chem. A* **2006**, *110*, 5735–5739.

(15) Fujitsuka, M.; Tojo, S.; Shinmyozu, T.; Majima, T. *Chem. Commun.* **2009**, 1553–1555.

(16) (a) Staab, H. A.; Zapf, U.; Gurke, A. *Angew. Chem., Int. Ed. Engl.* **1977**, *16*, 801–803. (b) Staab, H. A.; Zapf, U. *Angew. Chem., Int. Ed. Engl.* **1978**, *17*, 757–758. (c) Machida, H.; Tatemitu, H.; Otsubo, T.; Sakata, Y.; Misumi, S. *Bull. Chem. Soc. Jpn.* **1980**, *53*, 2943–2952. (d) Staab, H. A.; Feurer, A.; Hauck, R. *Angew. Chem., Int. Ed. Engl.* **1994**, *33*, 2428–2431. (e) Stabb, H. A.; Terecel, M.; Fischer, R.; Krieger, C. *Angew. Chem., Int. Ed. Engl.* **1994**, *33*, 1463–1466. (f) Staab, H. A.; Wahl, P.; Kay, K. Y. *Chem. Ber.* **1987**, *120*, 541–549. (g) Staab, H. A.; Krieger, C.; Wahl, P.; Kay, K. Y. *Chem. Ber.* **1987**, *120*, 551–558. (h) Tatemitu, H.; Natsume, B.; Yoshida, M.; Sakata, Y.; Misumi, S. *Tetrahedron Lett.* **1978**, *19*, 3459–3462. (i) Staab, H. A.; Knaus, G. H.; Henke, H. E.; Krieger, C. *Chem. Ber.* **1983**, *116*, 2785–2807. (j) Staab, H. A.; Hinz, R.; Knaus, G. H.; Krieger, C. *Chem. Ber.* **1983**, *116*, 2835–2847.

(17) Pesin, V. G.; D'yachenko, E. K. *Khim. Geterotsikl. Soed.* **1967**, *6*, 1048–1052.

SCHEME 1. Synthetic Routes to the Two- and Three-Layered [3.3]PCP **1** and **2** and the Selected <sup>1</sup>H NMR Data<sup>a</sup>

<sup>a</sup>Conditions: (a) *n*-Bu<sub>4</sub>NI, NaOH, CH<sub>2</sub>Cl<sub>2</sub>–H<sub>2</sub>O; (b) concd HCl; (c) KOH, H<sub>2</sub>NNH<sub>2</sub>·H<sub>2</sub>O, diethylene glycol. (**5**) Ha: 7.14, Hb: 6.83, Hc: 6.07. (**1**) Ha: 6.87, Hb: 6.79, Hc: 5.94. (**7**) Ha: 6.95, Hb: 6.92, Hc: 5.53, Hd: 5.99, He: 6.26, Hf: 6.47, Hg: 6.52, Hh: 6.46. (**2**) Ha: 6.67, Hb: 6.42, Hc: 5.40, Hd: 6.05, He: 6.30, Hf: 6.52, Hg: 6.47, Hh: 6.40.

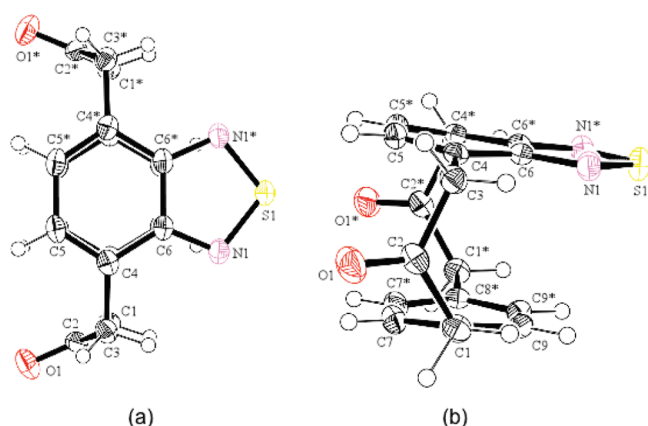


**FIGURE 1.** ORTEP drawing of the molecular structure of two-layered [3.3]PCP-dione **5** (–150 °C): top (a) and side (b) views.

increase, due to the ring current effect of the facing aromatic rings (Figures S1–S19, Supporting Information). The H<sub>a</sub>, H<sub>f</sub>, and H<sub>g</sub> proton signals are slightly deshielded compared to the corresponding protons of H<sub>b</sub>, H<sub>c</sub>, and H<sub>h</sub> due to the steric compression effect of the benzylic protons of the trimethylene bridges at the pseudogeminal position in the three-layered [3.3]PCPs.<sup>8a</sup> All of the H<sub>c</sub> and H<sub>e</sub> protons are strongly shielded due to the diamagnetic ring current effect of the facing BTD ring.<sup>13</sup>

**X-ray Structural Analysis.** Figure 1 shows the molecular structure of the two-layered PCP-dione **5** (–150 °C). The [3.3]PCP-dione unit takes a boat conformation in which the benzene and BTD rings are completely overlapped but slightly tilted (4.4°) with their average transannular distance of 3.28 Å. Interestingly, the two carbonyl groups are oriented opposite (anti) to the BTD ring. In the crystal-packing diagram of **5** (Figure 2), the intermolecular hydrogen bond between a methylene hydrogen atom of the bridge and the

oxygen atom of the carbonyl group [O1–H1 (2.550 Å)] (Figure 2A), as well as the CH/π interactions, are observed along the *c*-axis [C6–H5 (2.883 Å and 2.877 Å)] (Figure 2B), which are shorter than the sum of the van der Waals radii of the hydrogen (1.20 Å) and oxygen atoms (1.60 Å) or carbon atom (1.70 Å).<sup>18</sup>

Figure 3 shows the molecular structure of the two-layered PCP **1** (–150 °C). The trimethylene bridges take a boat conformation with –CH<sub>2</sub>– pointing toward the BTD ring. The benzene and BTD rings are completely overlapped in an almost parallel fashion with the tilt of 1.5° and an average transannular distance of 3.20 Å. In the crystal packing diagram of **1** (Figure 4), an interaction between sulfur and aromatic hydrogen atoms is expected because of the shorter distances (S1–H16: 2.965 Å) than the sum of the van der Waals radii of sulfur (1.80 Å) and hydrogen (1.20 Å) atoms.<sup>18</sup>

Figure 5 shows the molecular structure (ORTEP drawing) of the (*R*)-isomer of the three-layered PCP **2**, which crystallized as a racemate. The three aromatic rings are completely stacked. The tilt and the average transannular distance between the BTD ring and the central benzene ring are 2.1° and 3.19 Å, whereas those between the two benzene rings are 1.0° and 3.26 Å, respectively. In the crystal packing diagram of **2** (Figure 6), the CH/π interaction of the benzene ring with the methylene hydrogen between the (*R*)/(*S*) isomers (2.894 Å), as well as the S···H interactions [S1–H1 (2.893 Å) and S1–H28 (2.994 Å)] between the sulfur atom and a benzylic hydrogen atom of the trimethylene bridge are observed. The crystallographic data and refinement details of **1**, **2**, and **5** are summarized in Table S1, Supporting Information.

The [3.3]PCP-dione **5** takes a boat<sub>anti</sub> conformation (**5B-anti**), in which anti denotes the opposite direction of the bridges toward the BTD ring, probably in order to avoid any

(18) Pauling, L. *The Nature of the Chemical Bonds*; Cornell University Press: Ithaca, NY, 1960; p 260.

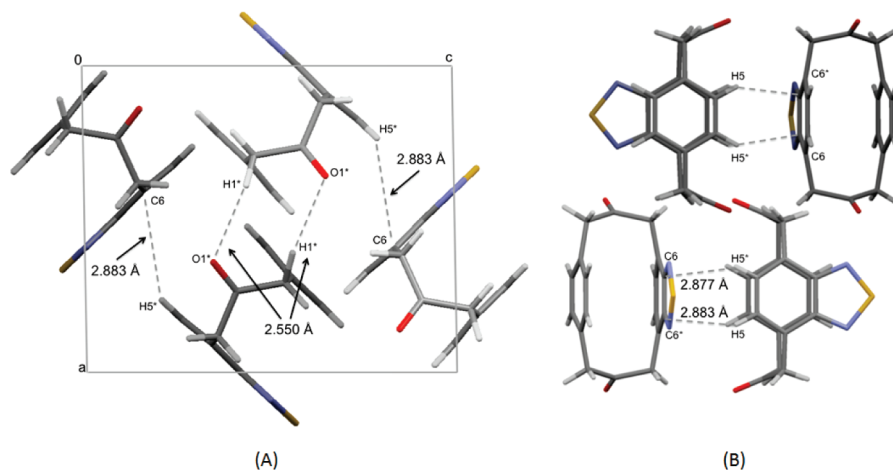


FIGURE 2. Crystal packing diagram of the two-layered [3.3]PCP-dione **5** ( $-150\text{ }^{\circ}\text{C}$ ).

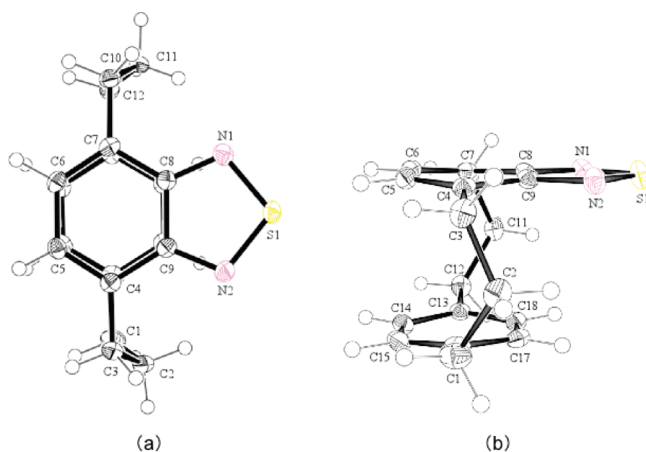


FIGURE 3. ORTEP drawing of the molecular structure of the [3.3]PCP **1** ( $-150\text{ }^{\circ}\text{C}$ ): top (a) and side (b) views.

electronic repulsion between the oxygen atom of the carbonyl group and the nitrogen atom of the BTD ring. The B3LYP/6-31G(d)<sup>19</sup> calculations (Gaussian 03)<sup>20</sup> better optimized the boat<sub>anti</sub> conformer (**5B-anti**) than the chair (**5C**) and boat (**5B**) conformers (Figure 7a), and this is in good agreement with the molecular structure in the solid state. In sharp contrast, the [3.3]PCP **1** takes a boat conformation in the solid state, in which the bridges are directed toward the BTD ring (**1B**, Figure 7b), probably due to the weak attrac-

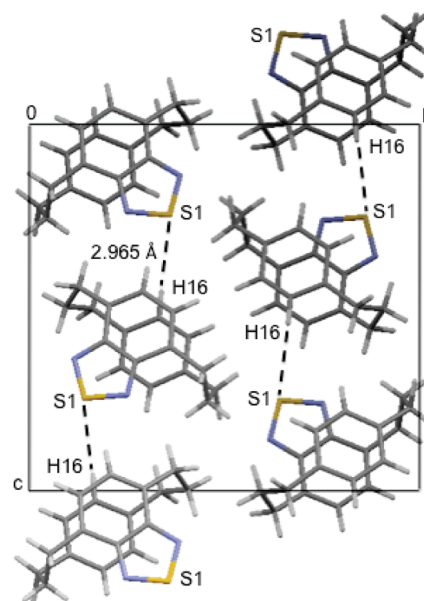


FIGURE 4. Crystal packing diagram of the [3.3]PCP **1** ( $-150\text{ }^{\circ}\text{C}$ ).

tive electronic interaction between the axial hydrogen atom at the central carbon of the trimethylene bridge and the nitrogen lone pair electrons of the BTD ring (Figure 8). In fact, one of the  $\text{H}_{\text{ax}} \cdots \text{N}$  distances ( $\text{H}_{\text{ax}1} - \text{N}1$ :  $2.684\text{ \AA}$ ,  $\text{H}_{\text{ax}2} - \text{N}2$ :  $2.622\text{ \AA}$ ), as shown by the crystal structure of **1**, is short enough to operate an attractive electronic interaction via intramolecular hydrogen bonds<sup>21,22</sup> because of the shorter distance than the sum of van der Waals radii of a hydrogen ( $1.11\text{ \AA}$ ) and nitrogen atoms ( $1.53\text{ \AA}$ ).

The three-layered [3.3]PCP **2** takes the boat/chair<sub>anti</sub> conformation (**2BCa**) in the solid state (Figure 5). Among the possible 16 conformations, the boat forms (**2BB**, **2BC**, **2BCa**, **2BBa**) of the [3.3]PCP moiety with a BTD ring are predicted to be more stable than the chair and boat<sub>anti</sub> conformers (Figure 9). Although the B3LYP/6-31G(d) calculations optimized **2BCa** to be slightly less stable than **2BB**, **2BCa** was

(19) (a) Becke, A. D. *J. Chem. Phys.* **1993**, *98*, 5648–5652. (b) Lee, C.; Yang, W.; Parr, R. G. *Phys. Rev. B* **1988**, *37*, 785–789. (c) Miehlich, B.; Savin, A.; Stoll, H.; Preuss, H. *Chem. Phys. Lett.* **1989**, *157*, 200–206.

(20) Frisch, M. J.; Trucks, G. W.; Schlegel, H. B.; Scuseria, G. E.; Robb, M. A.; Cheeseman, J. R.; Montgomery, J. A., Jr.; Vreven, T.; Kudin, K. N.; Burant, J. C.; Millam, J. M.; Iyengar, S. S.; Tomasi, J.; Barone, V.; Mennucci, B.; Cossi, M.; Scalmani, G.; Rega, N.; Petersson, G. A.; Nakatsuji, H.; Hada, M.; Ehara, M.; Toyota, K.; Fukuda, R.; Hasegawa, J.; Ishida, M.; Nakajima, T.; Honda, Y.; Kitao, O.; Nakai, H.; Klene, M.; Li, X.; Knox, J. E.; Hratchian, H. P.; Cross, J. B.; Bakken, V.; Adamo, C.; Jaramillo, J.; Gomperts, R.; Stratmann, R. E.; Yazyev, O.; Austin, A. J.; Cammi, R.; Pomelli, C.; Ochterski, J. W.; Ayala, P. Y.; Morokuma, K.; Voth, G. A.; Salvador, P.; Dannenberg, J. J.; Zakrzewski, V. G.; Dapprich, S.; Daniels, A. D.; Strain, M. C.; Farkas, O.; Malick, D. K.; Rabuck, A. D.; Raghavachari, K.; Foresman, J. B.; Ortiz, J. V.; Cui, Q.; Baboul, A. G.; Clifford, S.; Cioslowski, J.; Stefanov, B. B.; Liu, G.; Liashenko, A.; Piskorz, P.; Komaromi, I.; Martin, R. L.; Fox, D. J.; Keith, T.; Al-Laham, M. A.; Peng, C. Y.; Nanayakkara, A.; Challacombe, M.; Gill, P. M. W.; Johnson, B.; Chen, W.; Wong, M. W.; Gonzalez, C.; Pople, J. A. Gaussian 03, Revision C.02; Gaussian, Inc.: Wallingford, CT, 2004.

(21) Sako, K.; Tatemitsu, H.; Onaka, S.; Takemura, H.; Osada, S.; Wen, G.; Rudzinski, J. M.; Shinmyozu, T. *Liebigs Ann.* **1996**, 1645–1649.

(22) (a) Newkome, G. R.; Pappalardo, S.; Fronczek, F. R. *J. Am. Chem. Soc.* **1983**, *105*, 5152–5153. (b) Voegtle, F.; Koesgen, U. U.; Puff, H.; Reuter, H. *Chem. Ber.* **1989**, *122*, 343–346.

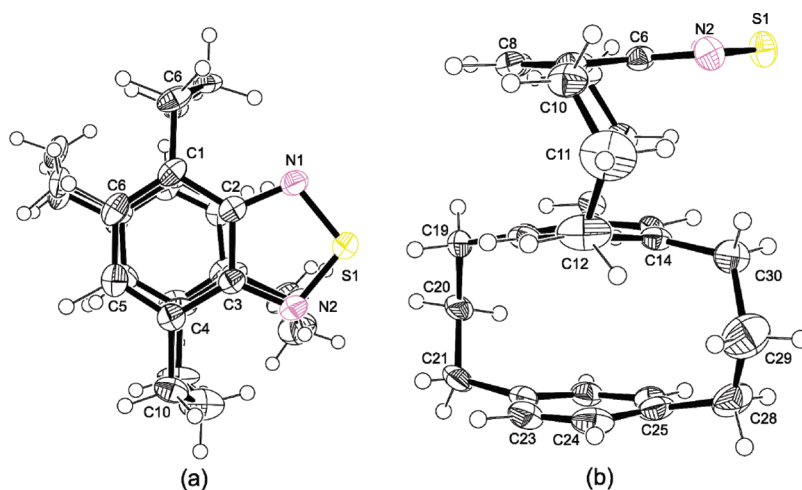


**FIGURE 5.** ORTEP drawing of the molecular structure of the (*R*)-isomer of the racemic three-layered [3.3]PCP **2** (−150 °C): top (a) and side (b) views.

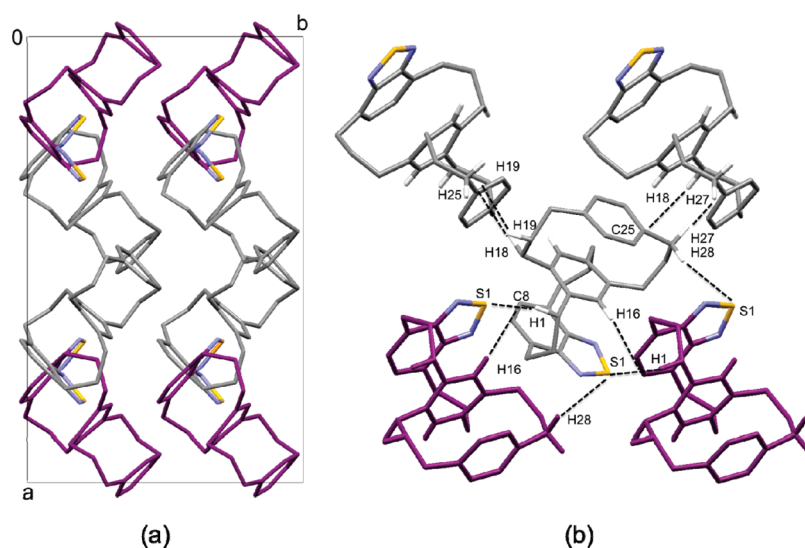


**FIGURE 6.** Crystal-packing diagram of the racemic three-layered [3.3]PCP **2** (−150 °C).

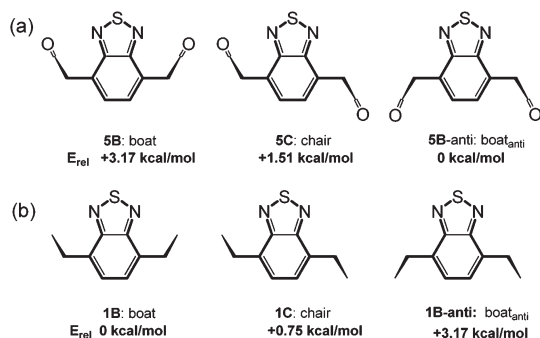


**FIGURE 7.** Possible conformers of the two-layered PCPs **5** (a) and **1** (b) at B3LYP/6-31G(d) level. The relative energies ( $E_{\text{rel}}$ ) are based on the total energies corrected with the zero-point vibrational energies.

actually observed in the crystalline state. However, the boat/boat conformation was observed for the crystal structure of the (*R*)-isomer of the parent three-layered [3.3]PCP.<sup>8b</sup>

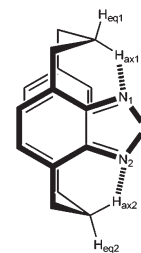


**FIGURE 8.** Possible  $H_{\text{ax}} \cdots N$  interaction in the boat conformation (**1B**) of **1**:  $H_{\text{ax1}}-N1$ , 2.684 Å;  $H_{\text{ax2}}-N2$ , 2.622 Å in the solid state at −150 °C.

All the tilts and the transannular distances between the two aromatic rings in **1**, **2**, and **5** are shorter than the corresponding tilts and distances of the parent two- and three-layered [3.3]PCPs (Table 1),<sup>8a,23</sup> suggesting the presence of significant intramolecular CT interaction.<sup>24</sup>

(23) Gantzel, P. K.; Trueblood, K. N. *Acta Crystallogr.* **1965**, *18*, 958–968.

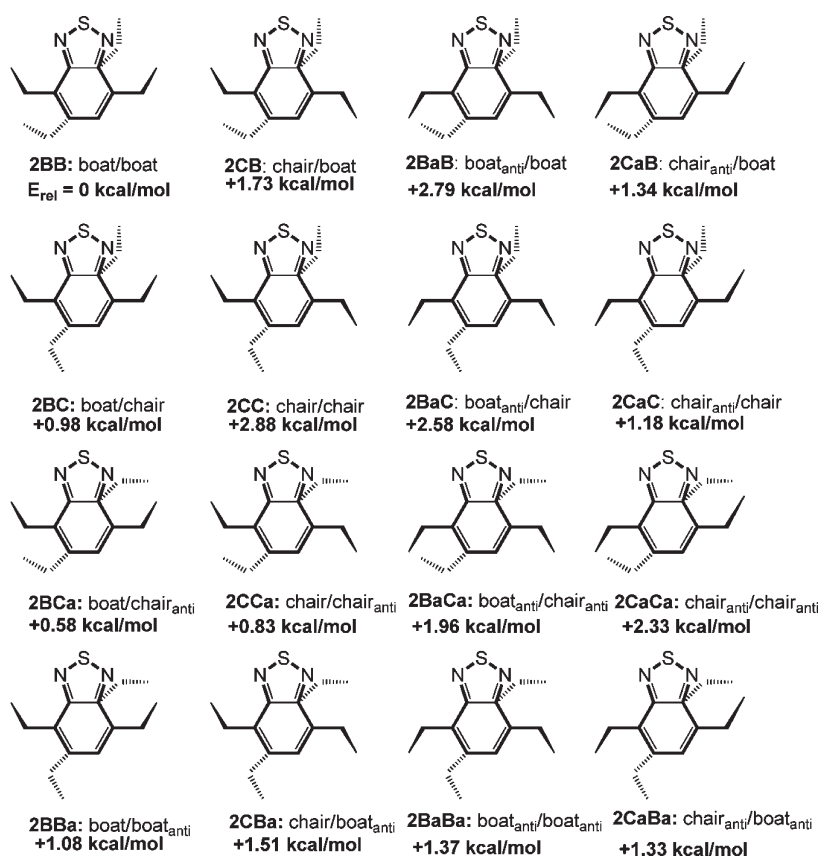


**FIGURE 9.** Possible conformers of **2** at the B3LYP/6-31G(d) level. The relative energies ( $E_{rel}$ ) are based on the total energies corrected with the zero-point vibrational energies.

**TABLE 1.** Summary of the Tilts and Transannular Distances of the Two- and Three-Layered [3.3]PCPs

compd	tilt (deg)	$r_{DA}$ (Å)
<b>1</b>	1.5	3.20
<b>2</b>	2.2, <sup>a</sup> 1.0 <sup>b</sup>	3.19, <sup>a</sup> 3.26 <sup>b</sup>
<b>5</b>	4.4	3.28
[3.3]PCP	0	3.25
three-layered[3.3]PCP	4.1, 4.3	3.26, 3.25
[3.3]PCP-dione	0	3.28
three-layered[3.3]PCP-dione	5.0, <sup>c</sup> 3.4 <sup>b</sup>	3.31, <sup>c</sup> 3.28 <sup>b</sup>

<sup>a</sup>Benzothiadiazole–benzene moiety. <sup>b</sup>[3.3]PCP moiety. <sup>c</sup>[3.3]PCP-dione moiety.

Regrettably, we have not yet succeeded in attaining good single crystals of the racemic three-layered [3.3]PCP-dione **7** for X-ray structural analysis and assessment of CT interaction relating to the tilt and the transannular distance shown in Table 1. All our attempts have been in vain because of severe disorder of the crystal structure (Table S2, Supporting Information). Recourse of the resolution of racemic **7** into a pair of enantiomers for X-ray structural analysis of individual enantiomer is currently in progress. Along this line, theoretical calculations [B3LYP/6-31G(d)] were carried out, which predicted that the boat<sub>anti</sub>/boat<sub>anti</sub> conformer (**7BaBa**) is most stable one among the 16 possible conformers (see Figure S39, Supporting Information).

**Electrochemical Properties.** In order to study the electronic properties of the D–A PCPs, cyclic voltammograms (CV) of

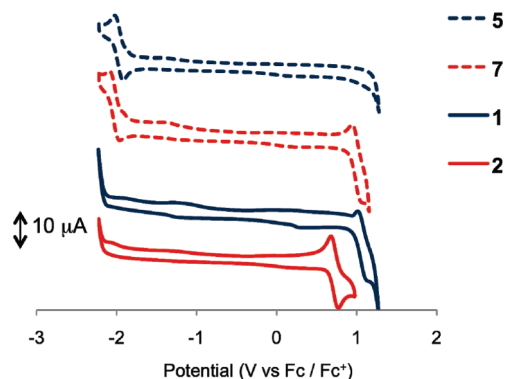


**FIGURE 10.** Cyclic voltammograms of the two- and three-layered [3.3]PCPs **1** and **2** and their respective diones **5** and **7** in  $\text{CH}_2\text{Cl}_2/0.1 \text{ M Bu}_4\text{NPF}_6$  observed at a potential scan rate of  $100 \text{ mV s}^{-1}$ .

the two- and three-layered PCPs, **5**, **7**, **1**, and **2**, were measured in  $\text{CH}_2\text{Cl}_2/\text{Bu}_4\text{NPF}_6$  (0.1 M) vs  $\text{Fc}/\text{Fc}^+$  (Figure 10). The resultant redox potentials are summarized in Table 2 with their HOMO and LUMO energies calculated by the DFT [MP2/6-31G(d)]<sup>25</sup> calculations (Gaussian 03) (Table S3, Supporting Information). The two-layered PCP-dione **5** shows a reversible one-electron reduction [ ${}^{\text{red}}E_{1/2}(\text{I})$ :  $-1.97 \text{ V}$ ] due to the generation of the radical anion species of the BTD ring because the value is similar to that of BTD [ ${}^{\text{red}}E_{1/2}(\text{I})$ :  $-1.98 \text{ V}$ ]. The two-layered PCP **1** exhibits an oxidation

(24) Furo, T.; Mori, T.; Wada, T.; Inoue, Y. *J. Am. Chem. Soc.* **2005**, *127*, 8242–8243.

(25) Head-Gordon, M.; Pople, J. A. *Chem. Phys. Lett.* **1988**, *153*, 503–506.

TABLE 2. Redox Potentials in CH<sub>2</sub>Cl<sub>2</sub> and the Calculated HOMO–LUMO Energies

compd	<sup>red</sup> $E_{1/2}(I)^a$ (V vs Fc/Fc <sup>+</sup> )	<sup>ox</sup> $E_{1/2}(I)^a$ (V vs Fc/Fc <sup>+</sup> )	<sup>ox</sup> $E_{pa}(I)^a$ (V vs Fc/Fc <sup>+</sup> )	LUMO <sup>c</sup> (eV)	HOMO <sup>c</sup> (eV)
<b>5</b>	−1.97 (−2.00) <sup>b</sup>			0.43	−8.15
<b>7</b>	−2.03 (−2.04) <sup>b</sup>	1.01	1.08	0.53	−7.42
<b>1</b>	(−2.26) <sup>b</sup>	1.08	1.14	1.04	−7.46
<b>2</b>	(−2.31) <sup>b</sup>	0.72	0.77	1.11	−6.97
[3.3]PCP			1.07	3.29	−7.35
three-layered [3.3]PCP (racemic)		0.64	0.66	3.37	−6.85
2,1,3-benzothiadiazole (BTD)	−1.98			0.84	−8.69

<sup>a</sup>Measured in CH<sub>2</sub>Cl<sub>2</sub>/0.1 M Bu<sub>4</sub>NPF<sub>6</sub> at the potential scan rate of 100 mV s<sup>−1</sup>. <sup>b</sup>Measured in THF/0.1 M Bu<sub>4</sub>NPF<sub>6</sub> at the potential scan rate of 100 mV s<sup>−1</sup>. <sup>c</sup>DFT (MP2/6-31G(d) level) calculations. The most optimized conformations (**5B**-anti, **7BaBa**, **1B**, **2BB**) as well as the boat and boat/boat conformations of the parent [3.3]PCP (ref 8a) and three-layered [3.3]PCP (ref 8c) were used, respectively, for the HOMO and LUMO calculations.

process [<sup>ox</sup> $E_{1/2}(I)$ : 1.08 V]. The value is comparable to that of the parent [3.3]PCP [<sup>ox</sup> $E_{1/2}(I)$ : 1.07 V], attributable to the process of generating the radical cation species of the [3.3]PCP moiety.<sup>26</sup> In sharp contrast, the three-layered PCP-dione **7** shows a reversible one-electron reduction [<sup>red</sup> $E_{1/2}(I)$ : −2.03 V] as well as a reversible one-electron oxidation [<sup>ox</sup> $E_{1/2}(I)$ : 1.01 V], suggesting the generation of a radical anion species of the BTD moiety and a radical cation species of the [3.3]PCP moiety, respectively.<sup>27</sup> The three-layered PCP **2** exhibited a reversible one-electron oxidation process with an oxidation potential [<sup>ox</sup> $E_{1/2}(I)$ : 0.72 V] much lower than that in **7**.<sup>28</sup> These results indicate that the presence of the −CH<sub>2</sub>COCH<sub>2</sub>− bridge interferes with the electronic interaction between the BTD and the [3.3]PCP moieties in **7**, whereas the transannular electronic interaction is effective in the presence of the −CH<sub>2</sub>CH<sub>2</sub>CH<sub>2</sub>− bridge in **2**.

In **1** and **2**, the oxidation process prevails and the oxidation potential decreases as the number of layer increases,<sup>8a</sup> and this is suggested by the higher LUMO energy in **2** than in **1** due to the more significant CT interaction between the BTD ring and the benzene rings in **2**.

As shown in Table 2, the HOMO energy is lower in **1** (−7.46 eV) but higher in **2** (−6.97 eV) than that of the [3.3]PCP (−7.35 eV), while the LUMO energy is higher both in **1** (1.04 eV) and **2** (1.11 eV) than that of BTD (0.84 eV). The two-layered PCP-dione **5** has very low HOMO (−8.15 eV) and LUMO (0.43 eV) energies, and this corresponds to the fact that **5** shows only the reduction process for the BTD ring. In contrast, **7** has HOMO energy (−7.42 eV) comparable to that of the [3.3]PCP and LUMO energy (0.53 eV) lower than that of BTD in good agreement with the fact that both the reduction and oxidation processes are observed in **7**. The CV study indicated the presence of a significant donor–acceptor interaction between the BTD ring and the benzene rings in **1** and **2**, whereas a very weak interaction is expected in **5** and **7**.

**UV/vis and Fluorescence Spectra.** Figure 11 shows the UV/vis spectra of **5**, **7**, **1**, and **2** in cyclohexane. The two-layered

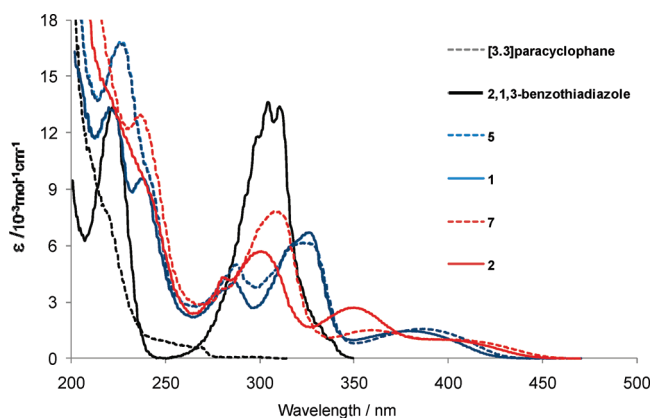


FIGURE 11. UV/vis spectra of the multilayered [3.3]PCPs in cyclohexane ( $1.0 \times 10^{-4}$  M).

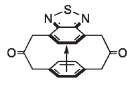
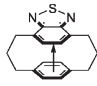
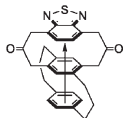
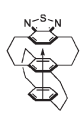
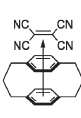
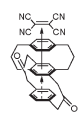
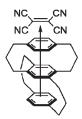
PCP-dione **5** exhibits three absorption bands at 288 (log  $\epsilon$  3.70), 325 (log  $\epsilon$  3.79), and 384 nm (log  $\epsilon$  3.20) beyond 250 nm, whereas **7** displays four absorption bands at 285 (sh, log  $\epsilon$  3.59), 308 (log  $\epsilon$  3.89), 360 (log  $\epsilon$  3.18), and 401 nm (log  $\epsilon$  3.01). The longest wavelength absorption band is assigned to the CT band because the band was not observed in the parent [3.3]PCP [267 nm (log  $\epsilon$  3.86)] and BTD [311 nm (log  $\epsilon$  5.12)] and the CT bands did not show any concentration dependence (Figures S31–S34, Supporting Information). The three-layered PCPs [**2**: 402; **7**: 401 nm] show more significant CT interaction than the two-layered PCPs [**1**: 378; **5**: 384 nm] in cyclohexane, as is expected by the smaller HOMO–LUMO gaps in the former than in the latter. It should be noted that the two-layered PCPs **1** [287 (log  $\epsilon$  3.61), 327 (log  $\epsilon$  3.82), 378 nm (log  $\epsilon$  3.16)] and **5** show similar absorption bands, and the similarity is also observed for **2** [281 (log  $\epsilon$  3.64), 301 (log  $\epsilon$  3.76), 350 (log  $\epsilon$  3.43), 402 (log  $\epsilon$  3.00)] and **7**. This phenomenon indicates that the intramolecular CT interaction is mainly responsible for the through-space electronic interaction between the A and D moieties in the two- and three-layered [3.3]PCPs, in sharp contrast to our previous observation that the presence of the −CH<sub>2</sub>COCH<sub>2</sub>− bridge interferes the electronic interaction between the BTD and the [3.3]PCP moieties in the redox properties in **7**. The positions of the CT bands and the calculated energy gaps between the HOMO of the donor and the LUMO of the acceptor in the intramolecular CT cyclophanes **1**, **2**, **5**, and **7** as well as the intermolecular CT complexes between the parent two- and three-layered [3.3]PCPs and TCNE in CHCl<sub>3</sub> are summarized in Table 3. A linear correlation between the CT interaction ( $h\nu_{CT}$ ) and the HOMO–LUMO gap was observed in the intramolecular CT cyclophanes and intermolecular CT complexes (Figure S35,

(26) Yasutake, M.; Koga, T.; Sakamoto, Y.; Komatsu, S.; Zhou, M.; Sako, K.; Tatemitsu, H.; Onaka, S.; Aso, Y.; Inoue, S.; Shinmyozu, T. *J. Am. Chem. Soc.* **2002**, *124*, 10136–10145.

(27) The CV profiles of the intermolecular CT complexes between the parent two- and three-layered [3.3]PCPs and TCNE show both oxidation process of the cyclophane moiety and reduction process of TCNE (Figures S28 and S29, Supporting Information). The oxidation potentials of the [3.3]PCP moieties of the complexes are similar to the corresponding oxidation potentials of the free [3.3]PCPs, suggesting the very weak electronic interaction between the [3.3]PCPs and TCNE under the conditions.

(28) Although **1** and **2** did not show any reduction process for the BTD ring in a CH<sub>2</sub>Cl<sub>2</sub> solution's potential window, the reduction process was observed in THF, in which **2** shows a higher reduction potential than **1** (Figure S30, Supporting Information).

**TABLE 3.** Positions of the CT Bands and the Calculated Energy Gaps of the HOMO of the Donor and the LUMO of the Acceptor in the Intramolecular CT Cyclophanes and Intermolecular CT Complexes in CHCl<sub>3</sub>

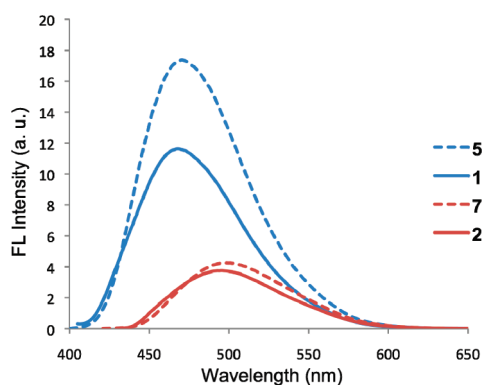
							
$\lambda_{CT}$ (nm)	384	384	404	402	606	594	670
$h\nu_{CT}$ (eV)	3.23	3.23	3.07	3.08	2.05	2.09	1.85
$\Delta E_{HOMO-LUMO}^a$ (eV)	8.58	8.56	7.99	8.13	5.58 <sup>b</sup>	5.53 <sup>b</sup>	5.09 <sup>b</sup>

<sup>a</sup>Optimized at the MP2/6-31G(d) level. <sup>b</sup>The energy difference between HOMO of [3.3]PCPs and LUMO of TCNE.

**TABLE 4.** UV/vis and Fluorescence Bands of Two- and Three-Layered [3.3]PCPs **1** and **2** ( $\lambda_{ext}$ : **5** and **1**, 379 nm; **7** and **2**, 392 nm)

compd	$\lambda_{max}/nm$ (log $\epsilon$ )			$\lambda_{flu}/nm$ ( $\Phi$ ) <sup>a</sup>		
	C <sub>6</sub> H <sub>12</sub>	CHCl <sub>3</sub>	MeCN	C <sub>6</sub> H <sub>12</sub>	CHCl <sub>3</sub>	MeCN
<b>1</b>	378 (3.16), 327 (3.82), 287 (3.61)	384 (3.16), 327 (3.84), 288 (3.61)	384 (3.12), 325 (3.80), 287 (3.56)	468 (0.51)	496 (0.49)	497 (0.19)
<b>2</b>	402 (3.00), 350 (3.43), 301 (3.76), 281 (3.64)	402 (3.03), 358 (3.44), 303 (3.81), 283 (3.69)	403 (2.99), 357 (3.40), 302 (3.75), 282 (3.64)	496 (0.12)	531 (0.08)	534 (0.02)
<b>5</b>	384 (3.20), 325 (3.79), 288 (3.70)	384 (3.20), 323 (3.78), 287 (3.72)	382 (3.16), 324 (3.76), 287 (3.65)	468 (0.85)	488 (0.68)	495 (0.45)
<b>7</b>	401 (3.01), 360 (3.18), 308 (3.89), 285 (3.59)	404 (3.00), 362 (3.19), 309 (3.89), 285 (3.62)	404 (2.98), 358 (3.22), 306 (3.85), 283 (3.62)	501 (0.13)	522 (0.05)	544 (0.01)

<sup>a</sup>Reference with fluorescein (0.97).

**FIGURE 12.** Fluorescence spectra of **1**, **2**, **5**, and **7** in cyclohexane ( $\lambda_{ext}$ : **5** and **1**, 379 nm; **7** and **2**, 392 nm).

Supporting Information). In the intermolecular CT complexes, the through-space interaction between the A and D moieties is also important.

Figure 12 shows fluorescence spectra of **5**, **7**, **1**, and **2** in cyclohexane, and all the UV/vis and fluorescence spectra are summarized in Table 4. The two-layered PCPs show broad, structureless fluorescent bands at the same positions [**5**: 468 nm ( $\Phi$  0.85); **1**: 468 nm ( $\Phi$  0.51)], and the quantum yield of **1** is lower than that of **5**. Similarly the three-layered dione **7** shows the band at 501 nm ( $\Phi$  0.13), which is comparable to that of **2** (496 nm,  $\Phi$  0.12). The positions and the intensities of these fluorescence bands did not show any concentration-dependence in the range of  $1.0 \times 10^{-5}$  to  $1.0 \times 10^{-6}$  mL<sup>-1</sup> (Figures S36–S38, Supporting Information). The fluorescence band of the parent [3.3]PCP appears at 360 nm in cyclohexane,<sup>29</sup> and BTD itself shows a fluorescence band at 402 nm in EtOH.<sup>13</sup> The broad fluorescent bands of **1** and **5** as

well as **2** and **7** may be attributed to the intramolecular exciplex emission. The longer wavelength and lower quantum yield for the CT band in the three-layered PCPs than those for the two-layered PCPs may be ascribed to the stronger intramolecular CT interaction in the ground state in the three-layered PCP. Large Stokes shifts were observed in the fluorescent spectra when the solvent polarity was changed. The fluorescent band shows a red-shift with an increase in the solvent polarity [**2**: 496 (cyclohexane), 531 (CHCl<sub>3</sub>), 534 nm (CH<sub>3</sub>CN)], and this effect is more significant in the [3.3]PCP-diones **5** and **7** than in the [3.3]PCPs **1** and **2** (Figures S36–S38, Supporting Information).

To estimate the excited state and the optical properties, TD<sup>30</sup>-DFT and TD-HF calculations of the two- and three-layered [3.3]PCPs **1** and **2** were examined by using the most stable conformations of **1B** and **2BB**, respectively, and the result is summarized in Table 5. The TD-DFT (B3LYP/6-31+G(d)//MP2/6-31G(d) and BHandHLYP<sup>31</sup>/6-31+G(d)//MP2/6-31G(d)) calculations predicted the longest absorption band of **1** at 471 and 391 nm, respectively, while TD-HF (B3LYP/6-31+G(d)//MP2/6-31G(d)) calculations predicted a much shorter wavelength at 343 nm. The position of the band calculated by the TD-BHandHLYP level well agrees with that of the observed one at 378 nm in cyclohexane. Similarly, the TD-BHandHLYP level calculations regenerate the observed position of the longest absorption band of **2** (calcd 418 nm, obsd 402 nm in cyclohexane), suggesting that the HOMO to LUMO transition (S1) contributes greatest to the longest absorption band of **2**.

Figure 13 includes the MO diagrams of **1** and **2** (BHandHLYP/6-31+G(d)//MP2/6-31G(d)),<sup>25</sup> in which the HOMO

(29) Nogita, R.; Matohara, K.; Yamaji, M.; Oda, T.; Sakamoto, Y.; Kumagai, T.; Lim, C.; Yasutake, M.; Shimo, T.; Jefford, C. W.; Shinmyozu, T. *J. Am. Chem. Soc.* **2004**, *126*, 13732–13741.

(30) (a) Stratmann, R. E.; Scuseria, G. E.; Frisch, M. J. *J. Chem. Phys.* **1998**, *109*, 8218–8224. (b) Bauernschmitt, R.; Ahlrichs, R. *Chem. Phys. Lett.* **1996**, *256*, 454–464. (c) Casida, M. E.; Jamorski, C.; Casida, K. C.; Salahub, D. R. *J. Chem. Phys.* **1998**, *108*, 4439–4449.

(31) Becke, A. D. *J. Chem. Phys.* **1993**, *98*, 1372–1377.



TABLE 5. Theoretical Calculation Results (Gas Phase) and the Observed Lowest Energy Absorption Bands in Cyclohexane

		excited state (contribution)	wavelength (nm)	excited energy (eV)	oscillator strength ( <i>f</i> )
1	B3LYP	HOMO → LUMO (0.67644)	471	2.63	0.0106
	BHandHLYP	HOMO → LUMO (0.67777)	391	3.17	0.0278
	HF	HOMO → LUMO (0.63894) HOMO -1 → LUMO (-0.24558)	343	3.61	0.0692
	exp		378	3.28	
2	B3LYP	HOMO → LUMO (0.68404)	533	2.33	0.0079
	BHandHLYP	HOMO → LUMO (0.63750) HOMO -1 → LUMO (0.22175) HOMO -2 → LUMO (-0.11474)	418	2.97	0.0186
	HF	HOMO → LUMO (0.52423) HOMO -1 → LUMO (-0.29453) HOMO -2 → LUMO (0.30222)	353	3.51	0.0575
	exp		402	3.08	

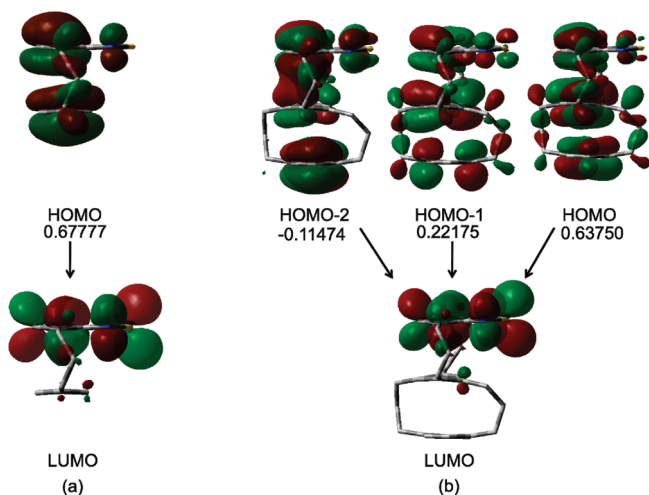


FIGURE 13. MO diagrams that contributed to the lowest excitation in **1** (a) and **2** (b) at the BHandHLYP/6-31+G(d)//MP2/6-31G(d) level.

orbitals are localized over the donor benzene moieties and benzo ring of the BTM moiety, while the LUMO orbital is localized over the acceptor BTM rings in both **1** and **2**. This suggests that the S1 state should have intramolecular CT character. Similar results were obtained in the diones **5** and **7** (Table S4, Supporting Information). The two- and three-layered [3.3]PCPs **1** and **2** have the dipole moments with same direction. The magnitude of their dipole moments is disclosed by calculations to be smaller in the excited state [**1**: 1.71 D, **2**: 1.81 D, BHandHLYP/6-31+G(d) level] than in the ground state [**1**: 1.95 D, **2**: 2.05 D, MP2/6-31G(d) level], suggesting more delocalized electronic structure in the excited state than in the ground state. This may be the reason for small Stokes shift observed in CH<sub>3</sub>CN. On the other hand, the magnitude of dipole moments of the diones **5** and **7** was predicted to be larger in the excited state [**5**: 3.70 D, **7**: 3.12 D] than in the ground state [**5**: 3.58 D, **7**: 3.04 D], supporting the experimental result that the fluorescent band shows red-shift as the solvent polarity increases (Table S5, Supporting Information). The positions of these fluorescence bands do not show any concentration dependence, suggesting that the Stokes shifts may be ascribed to the solvation effects of the S1 state.

### 3. Conclusions

As the first step in the study of the [3.3]PCP-based molecular wires with acceptor and donor moieties at terminals, we

synthesized the two- and three-layered [3.3]PCPs **1** and **2** containing BTM as an acceptor. The transannular distances between the aromatic rings of **1** and **2** are shorter than the corresponding distances in the parent two- and three-layered [3.3]PCPs due to the intramolecular CT interaction. The cyclic voltammograms of the two- and three-layered [3.3]PCPs **1** and **2** along with their respective diones **5** and **7** clearly indicate that the presence of the -CH<sub>2</sub>COCH<sub>2</sub>- bridge interferes with the electronic interactions between the BTM ring and the benzene rings, suggestive of the importance of the through-bond interaction along with the through-space interaction for the electronic interaction in the ground state. The CV study also suggests the generation of stable radical anion species for the two-layered dione **5** and radical cation species for the two- and three-layered PCPs **1** and **2**, whereas the generation of both the radical anion and radical cation species is expected in the three-layered dione **7**. In sharp contrast to the CV data, the UV/vis spectra exhibited bands similar to each other regardless of the presence of the -CH<sub>2</sub>COCH<sub>2</sub>- or -CH<sub>2</sub>CH<sub>2</sub>CH<sub>2</sub>- bridges, indicative of the importance of the through-space interactions between the A and D moieties in the excited state. The two-layered PCPs, **5** and **1**, show broad fluorescence bands at the same position (468 nm). However, fluorescence bands of the three-layered PCPs, **7** and **2**, appear, respectively, at 501 and 496 nm with lower quantum yields than those of the two-layered PCPs probably due to the presence of a strong intramolecular CT interaction in the ground state.

The pulse radiolysis and  $\gamma$ -ray irradiation studies of the radical anion and radical cation species in the two- and three-layered [3.3]PCPs may provide important information on the stabilities of the radical anion and the radical cation species, as well as the magnitude of the electron delocalization over the aromatic rings. Our preliminary study on the pulse radiolysis of the two- and three-layered [3.3]PCPs suggests the formation of cation radical species. The pulse radiolysis study of **1**, **2**, **5**, and **7**, as well as the study on their transient absorption spectra are in progress. In order to decrease the magnitude of the CT interaction in **2** in the ground state, we designed to connect the BTM moiety to an end of the multilayered [3.3]PCP by a single trimethylene bridge. Furthermore, the synthesis of A (BTM)-B (multilayered [3.3]PCP)-D (phenothiazine) system is also in progress and these results will be reported elsewhere.

### 4. Experimental Section

**Two-Layered [3.3]Paracyclophane, 1.** To a refluxing mixture of *n*-Bu<sub>4</sub>NI (0.84 g) and NaOH (8.2 g) dissolved in 32 mL of water and CH<sub>2</sub>Cl<sub>2</sub> (500 mL) was added dropwise a mixture

of the EbsMIC adduct **4** (4.46 g, 8.58 mmol) and the bis-(chloromethyl)benzothiadiazole **3** (2.00 g, 8.58 mmol) dissolved in  $\text{CH}_2\text{Cl}_2$  (250 mL) over a period of 7 h. The mixture was then refluxed for an additional 2 h. After cooling, the reaction mixture was washed with water and concentrated to a volume of ca. 200 mL. The concentrate was treated with concd HCl (30 mL) for 2 h at room temperature. The mixture was washed with brine, dried with  $\text{Na}_2\text{SO}_4$ , and concentrated to dryness to give the crude ketone, which was purified by silica gel column chromatography with  $\text{CH}_2\text{Cl}_2$  ( $R_f = 0.24$ ) to afford pure **5** (1.07 g, 36%) as yellow crystals. **5**: yellow needles ( $\text{CH}_2\text{Cl}_2/\text{EtOH}$ ); mp 183.5–184.5 °C; IR (KBr)  $\nu$  1698 (C=O)  $\text{cm}^{-1}$ ;  $^1\text{H}$  NMR (600 MHz,  $\text{CDCl}_3$ )  $\delta$  3.57 (d,  $J = 13.1$  Hz, 2H), 3.63 (d,  $J = 13.0$  Hz, 2H), 3.75 (d,  $J = 13.5$  Hz, 2H), 4.62 (d,  $J = 13.1$  Hz, 2H), 6.07 (s, 2H, ArH), 6.83 (s, 2H, ArH), 7.14 (s, 2H, ArH);  $^{13}\text{C}$  NMR (100 MHz)  $\delta$  47.7, 51.4, 125.1, 128.6, 129.2, 129.7, 134.0, 155.0, 204.7; HRMS (FAB)  $m/z$  calcd. for  $\text{C}_{18}\text{H}_{14}\text{N}_2\text{O}_2\text{S}$  322.0776 [ $\text{M}^+$ ], found 322.0777. Anal. Calcd for  $\text{C}_{18}\text{H}_{14}\text{N}_2\text{O}_2\text{S}$ : C, 67.06; H, 4.38; N, 8.69. Found: C, 66.81; H, 4.36; N, 8.72.

A mixture of the dione **5** (302 mg, 0.264 mol), 98%  $\text{NH}_2\text{NH}_2 \cdot \text{H}_2\text{O}$  (2.3 mL), KOH (1.55 g), and diethylene glycol (40 mL) was heated at 130 °C for 3 h and then at 200 °C for 3 h with stirring. After cooling, the mixture was poured into ice-water and extracted with  $\text{CH}_2\text{Cl}_2$ . The combined  $\text{CH}_2\text{Cl}_2$  extracts were washed with brine, dried with  $\text{Na}_2\text{SO}_4$ , and filtered. The filtrate was concentrated to dryness, and the resultant residue was purified by silica gel column chromatography with  $\text{CH}_2\text{Cl}_2/\text{hexane}$  (1:1,  $R_f = 0.50$ ) to give **1** (105 mg, 72%) as yellow crystals. **1**: yellow plates (pentane); mp 75.0–76.0 °C;  $^1\text{H}$  NMR (600 MHz,  $\text{CDCl}_3$ )  $\delta$  2.0–2.05 (m, 2H), 2.4–2.45 (m, 2H), 2.57–2.61 (m, 2H), 2.68–2.70 (m, 2H), 2.73–2.77 (m, 2H), 3.5–3.55 (m, 2H), 5.94 (s, 2H, ArH), 6.79 (s, 2H, ArH), 6.87 (s, 2H, ArH);  $^{13}\text{C}$  NMR (150 MHz)  $\delta$  26.9, 32.7, 35.4, 125.3, 129.8, 132.1, 138.4, 155.7; HRMS (FAB)  $m/z$  calcd. for  $\text{C}_{18}\text{H}_{18}\text{N}_2\text{S}$  294.1191 [ $\text{M}^+$ ], found 294.1190. Anal. Calcd for  $\text{C}_{18}\text{H}_{18}\text{N}_2\text{S}$ : C, 73.43; H, 6.16; N, 9.53. Found: C, 73.43; H, 6.16; N, 9.51.

**Three-Layered [3.3]Paracyclophane, 2.** To a refluxing mixture of *n*- $\text{Bu}_4\text{NI}$  (500 mg) and NaOH (10.5 g) dissolved in 25 mL of water and  $\text{CH}_2\text{Cl}_2$  (450 mL) was added dropwise a mixture of the EbsMIC adduct **6** (808 mg, 1.19 mmol) and the bis(chloromethyl)benzothiadiazole **3** (278 mg, 1.19 mmol) dissolved in  $\text{CH}_2\text{Cl}_2$  (250 mL) over a period of 8 h. The mixture was then refluxed for an additional 2 h. After cooling, the reaction mixture was washed with water and concentrated to a volume of ca. 100 mL. The concentrate was treated with concd HCl (20 mL) for 2 h at room temperature. The mixture was washed with brine, dried with  $\text{Na}_2\text{SO}_4$ , and filtered. The filtrate was concentrated to dryness to give the crude ketone, which was purified by silica gel column chromatography with  $\text{CH}_2\text{Cl}_2$  ( $R_f = 0.29$ ) to afford **7** as yellow crystals (213 mg, 37%). **7**: yellow needles (benzene); mp 230 °C dec; IR (KBr)  $\nu$  1699 (C=O)  $\text{cm}^{-1}$ ;  $^1\text{H}$  NMR (600 MHz,  $\text{CDCl}_3$ )  $\delta$  1.54–1.68 (m, 1H), 1.68–1.73 (m, 1H), 1.78–1.85 (m, 1H), 1.92–1.97 (m, 2H), 2.25–2.29 (m, 1H), 2.34–2.38 (m, 1H), 2.40–2.45 (m, 1H), 2.5–2.63 (m, 2H), 2.65–2.69 (m, 2H), 3.32 (d,  $J = 14.0$  Hz, 1H), 3.37 (d,  $J = 13.2$  Hz, 1H), 3.60 (d,  $J = 9.2$  Hz, 1H), 3.72 (d,  $J = 10.0$  Hz, 1H), 3.73 (d,  $J = 13.2$  Hz, 1H), 3.77 (d,  $J = 14.0$  Hz, 1H), 4.44 (d,  $J = 14.0$  Hz, 1H), 4.49 (d,  $J = 13.2$  Hz, 1H), 5.53 (s, 1H, ArH), 5.99 (s, 1H, ArH), 6.26 (d,  $J = 7.4$  Hz, 1H, ArH), 6.46 (d,  $J = 8.5$  Hz, 1H, ArH), 6.47 (d,  $J = 9.2$  Hz, 1H, ArH), 6.52 (d,  $J = 7.7$  Hz, 1H, ArH), 6.92 (d,  $J = 7.0$  Hz, 1H, ArH), 6.95 (d,  $J = 7.0$  Hz, 1H, ArH);  $^{13}\text{C}$  NMR (150 MHz,  $\text{CDCl}_3$ )  $\delta$  27.7, 28.3, 31.8, 33.7, 35.3, 35.7, 47.7, 48.1, 48.1 (overlapped) 50.1, 126.7, 127.1, 127.4, 127.9, 128.5, 128.6, 129.2, 130.0, 130.3, 131.1, 131.2, 132.6, 134.8, 137.8, 138.0, 138.03, 154.7, 155.1, 204.4, 205.6; HRMS (FAB)  $m/z$  calcd for  $\text{C}_{30}\text{H}_{28}\text{N}_2\text{O}_2\text{S}$  480.1872 [ $\text{M}^+$ ], found 480.1873. Anal. Calcd for  $\text{C}_{30}\text{H}_{28}\text{N}_2\text{O}_2\text{S}$ : C, 79.47; H, 5.87; N, 5.83. Found: C, 74.71; H, 5.87; N, 5.83.

A mixture of the dione **7** (231 mg, 0.481 mol), 98%  $\text{NH}_2\text{NH}_2 \cdot \text{H}_2\text{O}$  (0.7 mL), KOH (370 mg), and diethylene glycol (30 mL) was heated at 130 °C for 4.5 h and then at 200 °C for 2 h with stirring. After cooling, the mixture was poured into ice-water and extracted with  $\text{CH}_2\text{Cl}_2$ . The combined  $\text{CH}_2\text{Cl}_2$  solution was washed with brine, dried with  $\text{Na}_2\text{SO}_4$ , and filtered. The filtrate was concentrated to dryness and the resultant residue was purified by silica gel column chromatography with  $\text{CH}_2\text{Cl}_2/\text{hexane}$  (1:1,  $R_f = 0.50$ ) to give **2** (139 mg, 64%) as yellow crystals. **2**: yellow crystals (benzene); mp 208.0–209.0 °C;  $^1\text{H}$  NMR (600 MHz,  $\text{CDCl}_3$ )  $\delta$  1.53–1.6 (m, 1H), 1.65–1.73 (m, 2H), 1.85–1.95 (m, 4H), 2.24–2.27 (m, 1H), 2.3–2.45 (m, 2H), 2.5–2.63 (m, 3H), 2.65–2.69 (m, 2H), 2.8–2.88 (m, 2H), 3.38–3.43 (m, 2H), 5.40 (s, 1H, ArH), 6.05 (s, 1H, ArH), 6.30 (d,  $J = 7.4$  Hz, 1H, ArH), 6.40 (d,  $J = 7.5$  Hz, 1H, ArH), 6.47 (d,  $J = 7.6$  Hz, 1H, ArH), 6.52 (d,  $J = 7.8$  Hz, 1H, ArH), 6.62 (d,  $J = 6.8$  Hz, 1H, ArH), 6.67 (d,  $J = 6.8$  Hz, 1H, ArH);  $^{13}\text{C}$  NMR (150 MHz)  $\delta$  25.8, 26.0, 28.4, 28.5, 31.8, 32.7, 32.7 (overlapped), 32.8, 33.2, 33.4, 35.7, 35.9, 126.8, 127.1, 127.7, 129.4, 129.5, 129.6, 129.7, 131.66, 131.69, 133.4, 134.6, 135.6, 135.7, 135.8, 138.1, 138.14, 155.4, 155.7; HRMS (FAB)  $m/z$  calcd. for  $\text{C}_{30}\text{H}_{32}\text{N}_2\text{S}$  452.2286 [ $\text{M}^+$ ], found 452.2237. Anal. Calcd for  $\text{C}_{30}\text{H}_{32}\text{N}_2\text{S}$ : C, 79.47; H, 7.16; N, 6.19. Found: C, 79.60; H, 7.13; N, 6.19.

**X-ray Crystallographic Study.** Measurements were made using graphite-monochromated Mo K $\alpha$  ( $\lambda = 0.71069$  Å; radiation and a rotating anode generator). The crystal structures were solved by direct methods, [SIR97],<sup>32</sup> and refined by the full-matrix least-squares methods. The non-hydrogen atoms were anisotropically refined and hydrogen atoms were isotropically refined. The computations were performed using the teXan package.<sup>33</sup> Crystallographic data for the structural analyses of **1**, **5**, and **2** have been deposited to the Cambridge Crystallographic Data Centre (CCDC) as 762451, 762452, and 762453, respectively. Copies of this information may be obtained from The Director, CCDC, 12 Union Road, Cambridge CB2 1EZ, U.K. (Fax: +44 1223 336 033; e-mail: deposit@ccdc.cam.ac.uk) or <http://www.ccdc.cam.ac.uk/deposit>.

**Acknowledgment.** We thank the Theme Project (Professor Tahsin J. Chow), Institute of Chemistry, Academia Sinica, Taiwan R.O.C., for the financial support of this study. We also gratefully acknowledge financial support by a Grant-in-Aid for Scientific Research on Innovative Areas (No. 21106015) from the Ministry of Education, Culture, Sports, Science and Technology, Japan. Thanks are also due to Professor Teh-Chang Chou of Chaoyang University of Technology, Taiwan, for English correction of this manuscript. M.W. thanks the Venture-Business Laboratory, Kyushu University, for financial support through a Grant-in-Aid for Academic Challenge. M.W. also gratefully thanks Dr. Yuji Miyahara of the Department of Chemistry, Graduate School of Sciences, Kyushu University, for the sincere help and discussions throughout this study. The computations were carried out using the computer facilities at the Research Institute for Information Technology, Kyushu University.

**Supporting Information Available:** General experimental methods;  $^1\text{H}$ ,  $^{13}\text{C}$ , and 2D NMR spectra of **1–3**, **5**, and **7** (Figures S1–S26); cyclic voltammograms of the two- and three-layered [3.3]PCPs and BTD in  $\text{CH}_2\text{Cl}_2$  (Figure S27); cyclic voltammograms of the TCNE-multilayered [3.3]PCP complexes

(32) Altomare, A.; Burla, M. C.; Camalli, M.; Cascarano, G. L.; Giacovazzo, C.; Guagliardi, A.; Moliterni, A. G. G.; Polidori, G.; Spagna, R. *J. Appl. Crystallogr.* **1999**, *32*, 115–119.

(33) *Crystal Structure Analysis Package*; Molecular Structure Corp.: The Woodlands, TX, 1985, 1999.

(Figures S28 and S29 and Table S3), as well as **1**, **2**, **5**, and **7** in THF (Figure S30); UV/vis spectra (Figures S31–S35); HOMO–LUMO gap dependence on the peak position ( $h\nu_{CT}$ ) of the CT complex (Figures S36); fluorescence (Figures S37 and S38) spectra of **1**, **2**, **5**, and **7** in cyclohexane,  $\text{CHCl}_3$ , and MeCN; conformational analysis of **7** (Figure S39); summary of the crystallographic data and refinement details of **1**, **2**, **5**, and **7** (Tables S1 and S2);

summary of the calculated data of **1**, **2**, and **5** (Table S4); the TD-DFT and TD-HF results of **5** and **7** (Table S5); dipole moments calculations of **5**, **7**, **1**, and **2** (Table S6); calculated coordinate and total energies of optimized structures of **1**, **2**, **5**, **7**, PCPs, 2,1,3-benzothiadiazole, TCNE (Tables S7–S54), and CIF data of **1**, **2**, and **5** (Tables S55–S57). This material is available free of charge via the Internet at <http://pubs.acs.org>.